Northeastward growth of the Tibet plateau deduced from balanced reconstruction of two depositional areas- The Qaidam and Hexi Corridor basins, China

Francois Métivier, Yves Gaudemer, Paul Tapponnier, Bertrand Meyer

TECTONICS, VOL. 17, NO. 6, PAGES 823-842, DECEMBER 1998

Northeastward growth of the Tibet plateau deduced from balanced reconstruction of two depositional areas: The Qaidam and Hexi Corridor basins, China

François Métivier, Yves Gaudemer, Paul Tapponnier, and Bertrand Meyer

Laboratoire de Tectonique, Mécanique de la Lithosphère : URA 1093, Institut de Physique du Globe de Paris

Abstract. We address the problem of late Cenozoic uplift, erosion, and growth of northeastern Tibet by reconstructing, from isopach maps and drill holes, the volumes and masses of sediments deposited in the Qaidam and Hexi Corridor basins since $\sim$ 35 Myr ago. The mass budget is based on simple geometrical assumptions such as regional similarity of the thickness ratios between strata of different ages. In the Qaidam, where our record extends back to the Oligocene, the budget shows a huge rise of the accumulation rates after the beginning of the Pliocene (5.3 Ma). The early Pliocene seems to be the period of maximum deposition with accumulation rates in excess of 1 mm yr^{-1} ($\sim$ 2.7 kg m^{-2} yr^{-1}) of compacted rocks throughout the basin. There also seems to be a southeastward shift of the largest depocenters between the upper Pliocene (3.4 – 1.6 Ma) and the Quaternary. In the Hexi Corridor, sedimentation is confined to small foreland flexural depressions associated with the frontal thrusts of the Qilian Shan and occurs at an average rate one order of magnitude smaller than in the Qaidam basin. The accumulation rate is maximum in the Quaternary. The sedimentation history appears to support a plateau-building mechanism resulting from the combination of two geologicallly common processes: crustal-scale thrusting and sedimentary basin infilling. The time needed to completely fill the Qaidam basin and make its catchment a plateau closely resembling that of the highest part of Tibet (Qangtang) is of the order of 9 Myr. The mechanism now at work north of the Kunlun, which involves rapid infilling of broad, flat areas separated by relatively narrow mountain ranges, has thus probably been important in producing the high, smooth topography that characterizes much of central Tibet.

1. Introduction

The sedimentary record preserved in the basins that surround the mountains north of India may be used to constrain the mechanisms that have led to the rise of the Tibet plateau, whose deformation and uplift history has long been a subject of debate. The plateau covers an area of $\sim 2 \times 10^6$ km^2 with an average elevation of 5 km in its central and northern part (the Qangtang) [e.g., *Fielding et al.*, 1994].

Competing models invoked to account for its existence and rise imply markedly different modes of deformation of the mantle and crust. Wholesale underthrusting of India [*Argand*, 1924; *Powell and Conaghan*, 1973; *Ni and Barazangi*, 1983] requires that the Asian mantle be detached from its overlying crust by delamination [*Bird*, 1978]. Deformation of Asia as a viscous sheet [*England and McKenzie*, 1982; *England and Houseman*, 1986] implies widespread thickening of the Asian mantle north of the Himalayas. Convective removal of a lithospheric root underlying Tibet, a possible consequence of such mantle thickening, might lead to rapid and uniform rebound of a vast area to high elevation [*Molnar* et al., 1993], inducing sudden, regional climate change. Injection of the more resistant Indian crust into the weaker Asian crust, analogous to piston core injection [*Zhao and Morgan* 1985], might induce the rise of a high plateau by far-traveled flow of the lower crust alone. Thrusting on crustal-scale ramps above a large south dipping décollement along the north edge of the plateau [*Bally et al.*, 1986; *Mattauer*, 1986; *Tapponnier et al.*, 1990; *Meyer et al.*, 1998] is consistent with subduction of the Asian lithospheric mantle under the Kunlun. Elastic buckling [*Jin et al.*, 1994; *Burg et al.*, 1995] implies folding of the crust and mantle at two different wavelengths, which would also account for the topographic and crustal thickness variations observed in Tibet [*Hirn et al.*, 1984; *Wittlinger et al.*, 1996].

The deformation history and surface morphology that such models predict are also quite different. Some imply synchronous deformation and uplift over much of Tibet [e.g., *Zhao and Morgan*, 1985; *Molnar et al.*, 1993]; some imply propagation of deformation [*Powell and Conaghan*, 1973; *England and Houseman*, 1986; *Tapponnier et al.*, 1990; *Meyer et al.*, 1998], Others do not discriminate between these two possibilities [*Bird*, 1978; *Jin et al.*, 1994; *Burg et al.*, 1995]. Only two types of models [*Tapponnier et al.*, 1990 and *Meyer et al.*, 1998; *Jin et al.*, 1994; *Burg et al.*, 1995] address the

Paper number 98TC02764.
0278-7407/98/98TC-02764$12.00

"small-scale" topography of the plateau and possible variations of crustal thickness. The others are only concerned with the first-order flat topography, inferred to reflect uniform crustal thickness. Eventually, only one type of model takes erosion of reliefs and the existence of large sedimentary basins within the Tibet-Qinghai into account [*Meyer*, 1991; *Meyer et al.*, 1998].

Examination of present-day drainage in the Qangtang shows that it forms a mosaic of closed catchments with internal drainage, namely, sedimentary basins collecting the erosion products of nearby reliefs. The topography of NE Tibet, north of the Kunlun range, though different from that of the Qangtang in absolute elevation, exhibits strikingly similar features, with vast closed catchments feeding sedimentary basins that form flat plains surrounded by mountain ranges [*Meyer*, 1991; *Meyer et al.*, 1998](Plate 1). As a step toward understanding how the peculiar, current morphology of north central Tibet has formed, we therefore analyze here the interaction of tectonics and erosion in the desert-like regions north of the Kunlun where active mountain building and strong erosion are now in progress.

2. Coupled Sedimentation and Tectonics in NE Tibet

The Qaidam basin (Plate 1), whose surface, at an average elevation of 2700 m above sea level (asl), is covered with salt flats, extends over an area of 103,000 km^2 (Table 1) at the foot of the $\sim$ 6000-m-high Kunlun range. The catchment area of the basin (excluding the depositional area) covers 151,000 km^2 and extends from the Kunlun Shan to the Altyn, Tang He Nan, and Qinghai Nan Shan. A few streams only are perennial.

North of the Qilian Shan, on the Gobi-Ala Shan Platform, the Hexi Corridor basin stands $\sim$ 1400 m asl, $\sim$ 1300 m lower than the Qaidam. With a surface of 18,000 km^2 this narrow alluvial plain is mostly fed by rivers draining the Qilian mountains. The corresponding catchment area is about 38,000 km^2. The biggest perennial river is the Hei He, whose inland delta reaches into Mongolia.

Tertiary and Quaternary thrusting is particularly prominent north of the Kunlun fault. Plio-Quaternary folding and thrusting is clear on seismic sections [*Bally* et al., 1986]. At the foot of the Kunlun range, thrusts cut through the Oligo-Miocene deposits. Along the south side of the Qaidam the SW dipping thrusts remain hidden under thick Plio-Quaternary sediments [*Bally et al.*, 1986]. The traces of seismic, SW dipping thrusts have been mapped, using SPOT satellite imagery, topographic maps and field evidence along the foothills of the Tang-He Nan, Sule Nan, Qilian Shan and Long Shu Shan [*Tapponnier et al.*, 1990; *Meyer*, 1991 ; *Meyer et al.*, 1998]. NE dipping, active thrusts also exist along the Qinghai Nan Shan [*Van der Woerd et al.* 1998]. Scarps offsetting Quaternary fan surfaces are common along those thrusts, segments of which have produced large earthquakes (Luo Tuo Chen in 180 A.D., Chang Ma in 1932 (M =7.6), Gong He in 1990, (M=6.9), Gulang in 1927 (M=8.3)) [*Peltzer et al.*, 1989; *Gong et al.*, 1993; *Tapponnier et al.*, 1990; *Chen et al.*, 1994; *Gaudemer et al.*, 1995]. Most of the major thrust systems absorb $\sim$ N30°E shortening and have been active throughout the Quaternary at least (Fig 1).

The Altyn Tagh fault appears to control the geometry of mountain building in NE Tibet [e.g., *Peltzer et al.*, 1989; *Tapponnier et al.*, 1990; *Meyer*, 1991 ; *Meyer et al.*, 1998]. There is much less deformation west and north of the fault in the stable Tarim block than south and east of the fault, where the surface currently affected by thrusting and folding covers an area approximatively the size of the Tarim basin (more than 500,000 km^2, excluding the two sedimentary basins of interest in this study). Northeastward, there is little thrusting beyond the Long Shu Shan, not far from where the Altyn Tagh fault vanishes (Plate 1). Quaternary left-lateral slip on the Altyn Tagh and Kunlun faults appears to be kinematically coherent and in the case of the Altyn Tagh physically linked with thrusting in the Qilian ranges and in NE Tibet in general [*Meyer*, 1991; *Meyer et al.*, 1998].

Active tectonics and erosion-sedimentation are interdependent. Sustained uplift of a mountain range favors sustained river incision and erosion and leads to the formation of foreland flexural depressions. This has led *Tapponnier et al.* [1990], *Meyer* [1991] and *Meyer et al.* [1998] to propose that most of the parallel ranges in NE Tibet grew as large-scale ramp anticlines above

Table 1. Physiography of Drainage Areas of Qaidam, Hexi Corridor, and Gong He Basins

Basin	Depositional Area, km^2	Drainage Area, km^2	Base Level, m asl	Volume of Topography Above Base Level, km^3
Gong He	9,700	4,000	3,000	3,600
He Xi	18,000 (160,000)	37,900	1,400	71,000
Qaidam	103,300	150,800	2,700	205,300

Calculated from *Defense Mapping Agency* [1992]. Number in parentheses is Quaternary depositional area at time of change.

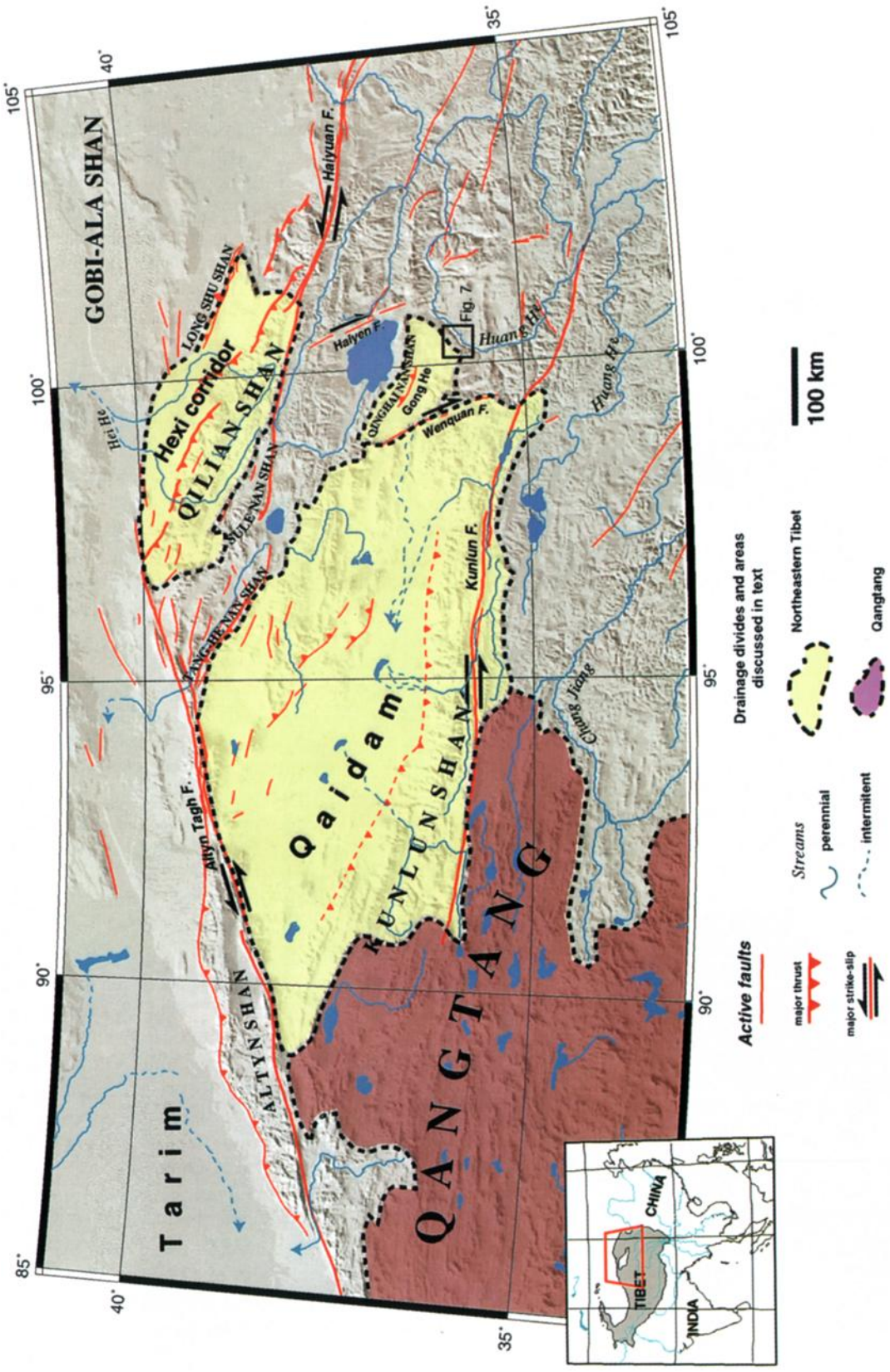

Plate 1. Location map of study area. Digital image of hypsography and rivers from *Defense Mapping Agency* [1992], active faults from *Meyer* [1991] and *Tapponnier et al.* [1986]. Note very sharp truncation of thrusts and ranges by left-lateral Altyn Tagh strike-slip fault. Box south of Gong He basin shows location of Figure 7.

south-dipping thrusts splaying from the left-lateral Altyn Tagh and Kunlun faults and that sediment accumulation in the basins caught between such rising ranges was an important process in the buildup of Tibet's high and flat topography. Figure 1 summarizes such a mechanism, which coinvolves thrusting and basin infilling. Fast migration of thrusting and crustal shortening is guided by the propagation of the Altyn Tagh fault, leading to the formation of distant, parallel, narrow ranges. As they grow, the ranges induce formation of flexural foredeeps that begin to fill with the erosion products derived from the adjacent mountains. As new ranges form farther northward near the tip of the propagating strike-slip fault, basins born as foredeeps progressively become captive. Ultimately, damming of the catchments outlets by active tectonic uplift and strike-slip faulting induces an increase of sedimentation within the basins that end up as piggyback basins and fill rapidly. The final result of such a coupling between tectonics and erosion is a morphology characterized by high flat and smooth surfaces separated by narrow mountain ranges, typical of that currently observed on the Tibet plateau.

In what follows, we discuss the mechanism outlined in Figure 1 using the sedimentary history of the Qaidam and Hexi basins since about 25 Ma. We perform a mass balance of the sediments deposited in these two basins and compare them with tectonic evidence for strike-slip faulting that closes catchments. The sediment data are derived from petroleum surveys while the structural data are derived from active tectonic and field studies. We therefore use two independant data sets to test the plausibility of the "catchment closure and basin infilling" mechanism. Eventually, we try to estimate the quantitative implications of such a mechanism in terms of timing for the growth of Tibet.

3. Data and Processing Technique

3.1. Stratigraphy of the Basins

Both the Qaidam and Hexi Corridor have Precambrian basements. The former, dated around 1.5–2 billion years [e.g., *Wang and Coward*, 1990, and references therein], is covered with alternating series of shallow marine and continental sediments of Paleozoic to Triassic age. The latter is covered with a series of marine deep water, progressively evolving into continental facies until the Permian, by the end of which the withdrawal of the sea is complete. In the Qaidam such withdrawal only takes place around the end of Triassic [*Bally et al.*, 1986; *Wang and Coward*, 1990, 1993]. Lacustrine Jurassic and Cretaceous rocks are then deposited along the NE margin of this basin. To the south such rocks progressively evolve to swamp deposits and to fluvial conglomerates, sandstones, and mudstones. Continental facies of lacustrine and fluvial type, alternately coarse (e.g., sandstones and conglomerates) and fine (e.g. mudstones and shales) also develop in the Hexi Corridor during the same period. Paleocene and Eocene deltaic and shallow lacustrine sandstones containing ostracods and plants, generally unconformable on the Mesozoic strata, remain confined to the NE border of the Qaidam (Lulehe Formation) and are absent in the Hexi Corridor. From the Middle Oligocene to the end of the Miocene, lacustrine, dark-colored argillaceous deposits invade the entire Qaidam (Ganchaigou Formation.), whereas the first Cenozoic sediments deposited in the corridor are of coarse type [*Xu*, 1985; *Wang and Coward*, 1993]. During the Pliocene, fluvial and lacustrine facies (Youshashan Formation) become dominant in the Qaidam [*Chen and Bowler*, 1986], and the salinity of distal deltaic lakes rises, as indicated by the presence of gypsum in shales and clay stones (Shizigou Formation) [*Xu*, 1985]. Sedimentation during that period in the Corridor is characterized by fluvial sandstones evolving into conglomerates. The Quaternary deposits of the Qaidam are chiefly composed of dark-colored, argillaceous, gypsum-bearing strata (Qigequan Formation), conglomerates and sandstones, while fluvial piedmont sediments are predominant in the corridor [e.g., *Xu*, 1985; *Gu and Di*, 1989; *Wang and Coward*, 1990, 1993].

Dating of continental strata is based on palynology and freshwater fossil assemblages. Some ages, especially that of the lower part of the Youshashan Formation, are subject to discussion. *Xu* [1985], on the basis of drill sections, dates this formation as middle to late Miocene, whereas other authors [e.g., *Bally et al.*, 1986; *Gu and Di*, 1989; *Bureau of Geology and Mineral Resources of Qinghai Province*, 1991] place the entire Youshashan Formation in the Pliocene. Since only *Xu* [1985] gives fossil assemblages resulting from detailed analysis of drill cores, we will thereafter consider that this formation is of late Miocene age or younger. Typical fossil assemblages corresponding to the Miocene and Pliocene formations are given in Table 2. Dating uncertainties are discussed in appendix B. We had access to eight drill logs in the Qaidam basin and four in the Hexi Corridor. Complete stratigraphy for the former is given by *Xu* [1985], while information on the latter was provided by the French petroleum company TOTAL CFP. Figure 2 shows a simplified stratigraphy of drill holes in the Qaidam area. Table 3 sums up stratigraphic information for the drill logs available, and Table 4 summarizes the data used to complete our mass balance for the Qaidam and Hexi Corridor. We also had access to several isopach maps: four in the Qaidam and two in the Hexi basin. As is usual in oil research and exploration, such maps are derived from linear interpolation between seismic sections and between calibration points obtained from drilling. Figure 3 shows the sampling of

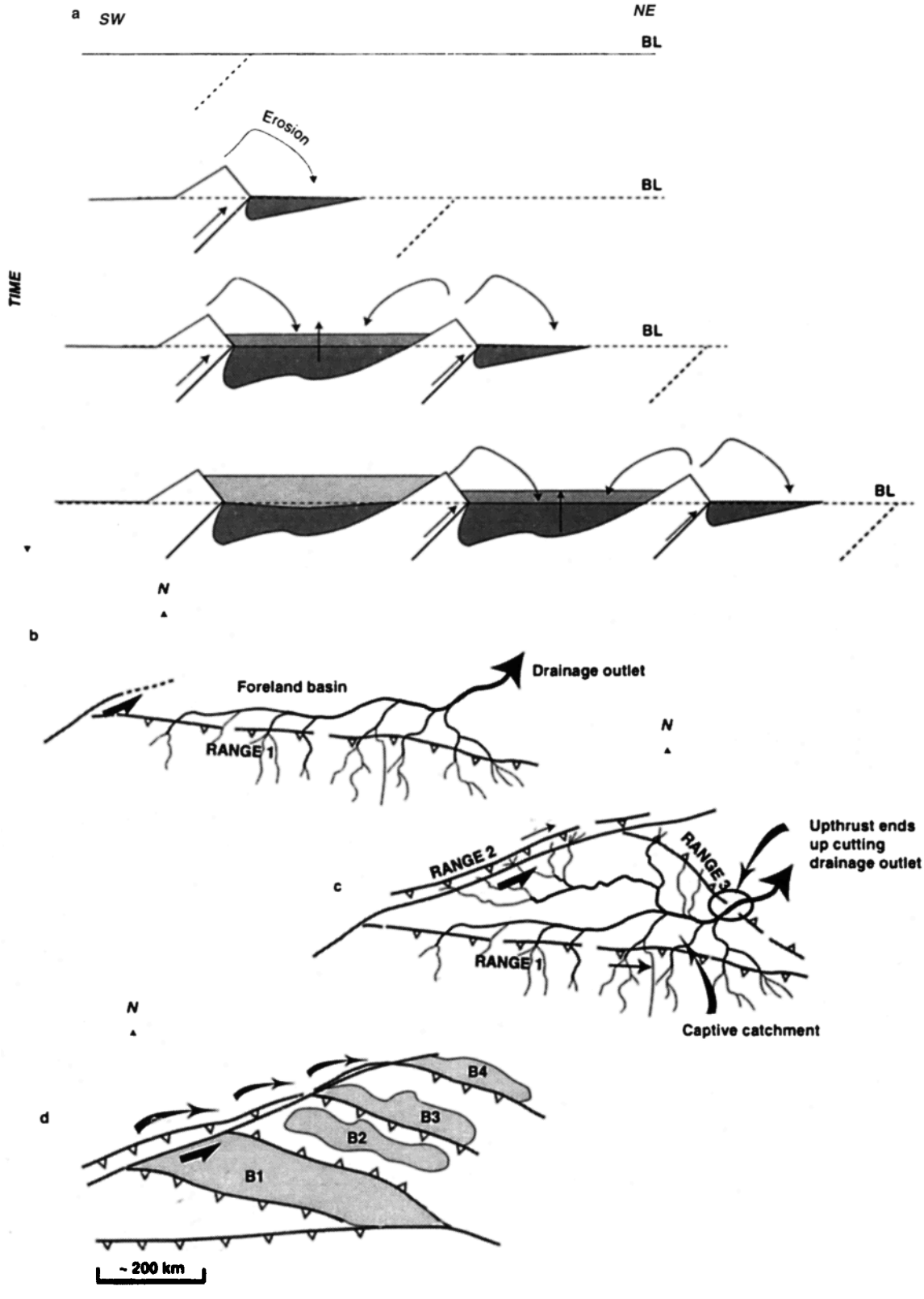

Figure 1. (a) Cross-sectional sketch showing proposed model of formation of a plateau by rise of successive ranges separated by foreland depressions whose drainage outlets become dammed, inducing rapid basin infill. (b) and (c) map view of same model at three different time intervals: (a) foreland depression (Figure 1a), becoming closed (Figure 1b) and filled with sediment (Figure 1c). This process results from uplift of surrounding mountain belts, induced by large-scale propagation of bounding strike-slip faults (Figure 1d).

Table 2. Palynological and Fossil Dating of Continental Strata in NE Tibet

Period	Formation	Palynology and Fossil Assemblages
Quaternary	Qigequan	*Stegodon orientalis* Owen
		Radix grabaui (Ping)
		R. plicatula (Benson)
		Eucypris inflata (Sars)
		Cyprinotus salinus (Brady)
		Cyprideis littoralis (Brady)
		Candona neglecta G. O. Sars
		Hyocypris bradyi G. O. Sars
Upper Pliocene	Shizigou	*Cyprideis torosa* (Jones)
		Hyocypris dorsotuberculata Chen Tian-min
		Eucypris concinna rostrata Sun Zhen-cheng
		Candona convexa qiulingensis Yang
Lower Pliocene	Upper Youshashan	*Planorbarius corneus* (Linnaeus)
		Planorbis procumbens Volkova
		Cyprideis littoralis (Brady)
		Candona kirgizica Mandelstam
		Tectochara mariai Globula
Miocene to Oligocene	Lower Youshashan Ganchaigou	*Planorbis youngi* Ping
		P. tungurensis Ping
		Candona kirgizica Mandelstam
		Cyprinotus derupta Schneider
		C. arguatus Schneider
		C. aff. *catillus* Schneider
		Cyprideis torosa Jones
		Eucypris longa Mandelstam
		E. aff. *oculata* Schneider
		Charites molassica (Straub)

The four fossil assemblages used to constrain the ages of our Cenozoic units are given by *Xu* [1985].

the isopachs. In order to maximize absolute errors in our calculation, we assumed, for each map available, an uncertainty equal to the contour interval. We also digitized isopachs of Quaternary deposits in the Gonghe basin, a smaller sedimentary basin east of the Qaidam, fed by the growing Qinghai Nan Shan and now incised by the Huang He (Plate 1). This latter map gives us information about the Quaternary infilling of a basin located east of the Qaidam and will later on be used for comparison purposes. All calculations linked with topographic volumes were made with 2 min of arc resolution digital elevation models (DEM) derived from the *Defense Mapping Agency* [1992].

3.2. Compacting Rocks to get Mass

The reconstruction technique used to produce a conservative mass balance of the volumes accumulated in the Qaidam basin has already been described by *Métivier and Gaudemer* [1997], but we summarize here the methodology because, unlike in usual back stripping analyses, the physical balance we perform implies studying compacted, rather than decompacted, strata in order to estimate the sediment mass [e.g., *Gallagher*, 1989; *Baldwin and Butler*, 1985].

Calculating mass from sediment thickness measurements implies that we know how density varies with depth. There are two ways of conducting such a calculation if the stratigraphic sequence $\{(z_i, t_i), i = 1, \ldots, N\}$ is known, each (z_i, t_i) pair defines the age (t_i) and the depth (z_i) of the ith strata, the first one being the youngest one, and if either the density $\rho(z)$ or the porosity $\omega(z)$ are known. Given depth and density, the mass accumulation M per unit area over a time interval Δt is

$$M(\Delta t) = \int_{z_1}^{z_2} \rho(z)\, dz \tag{1}$$

where z_1 and z_2 are the upper and lower limits of the strata deposited during time interval $\Delta t = t_2 - t_1$. This is the most precise way to obtain $M(\Delta t)$. The knowledge of $\rho(z)$ often being poor, one can derive the mass from the knowledge of porosity.

From depth and porosity, one can obtain the grain volume [*Gallagher*, 1989] which can be directly related to the mass by the grain density $\rho_g(z)$

$$M(\Delta t) = \int_{z_1}^{z_2} \rho_g(z)[1 - \omega(z)]\, dz \tag{2}$$

The grain density can be shown to be, on average, a constant $\overline{\rho}$ of order of 2.7×10^3 kg.m^{-3} [*Baldwin and Butler*, 1985; *Curray*, 1994; *Métivier*, 1996; *Métivier and Gaudemer*, 1997]. We shall use this average value noting that in the case of the Qaidam and Hexi basins, the composition of the sedimentary sequences excludes

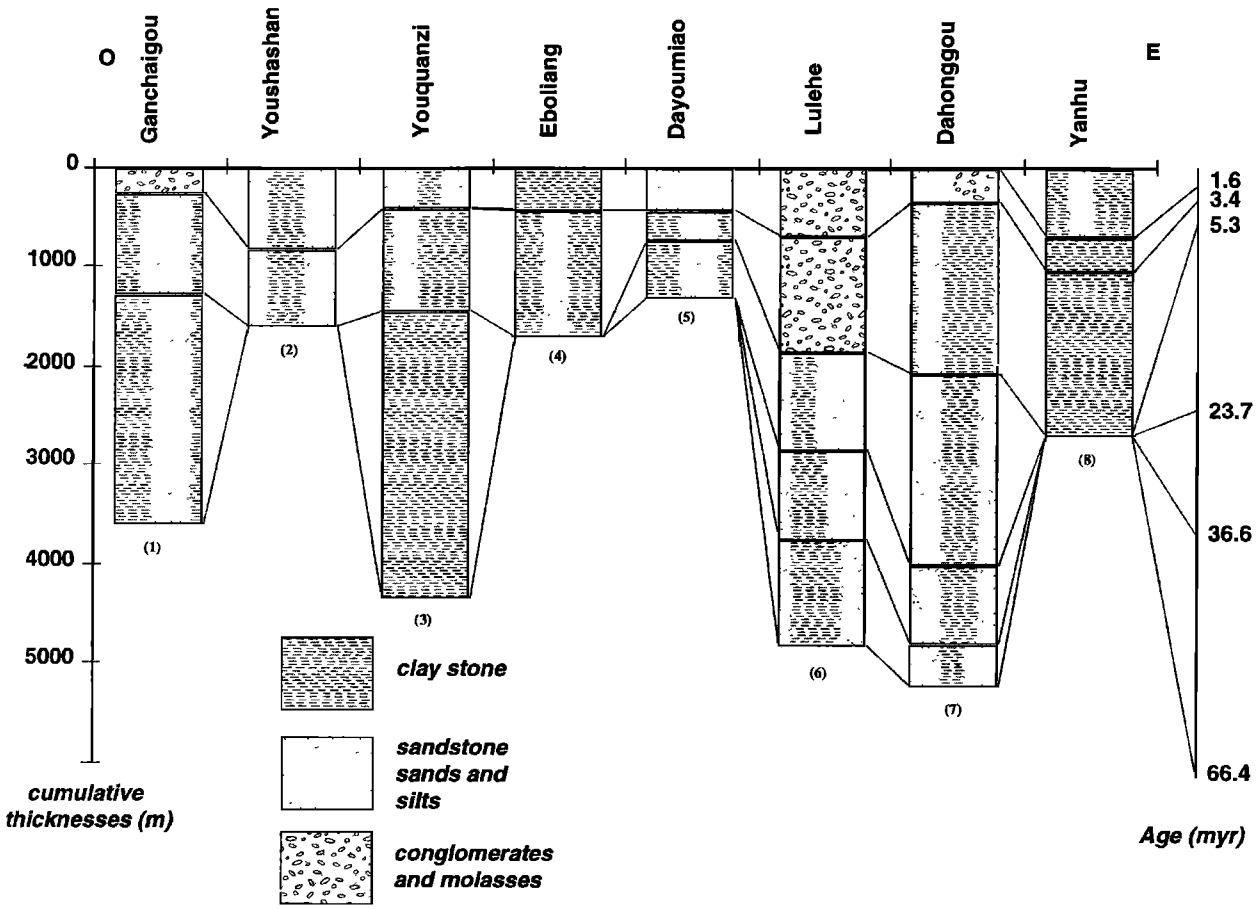

Figure 2. Simplified stratigraphic logs of Neogene sections in Qaidam basin. Locations and exact thicknesses are given in Table 3. Proportion of coarse and fine sediments in each log box corresponds approximately to real proportion in strata. Numbers refer to position on map of figure 3.

Table 3. Stratigraphic information Derived From Drill Logs in Qaidam and Hexi Corridor Basins.

	Location		Tertiary Cumulative Thicknesses, m				
	Longitude	Latitude	Upper Pliocene	Lower Pliocene	Miocene	Oligocene	Paleocene
Qaidam Basin							
Lulehe	94.7	38	700	1850	2850	3750	4825
Dahonggou	95	37.4	350	2075	4000	4800	5225
Yanhu	95.1	37.1	1050	2700	-	-	-
Ganchaigou	90.7	38.5	275	1275	3600		
Youshashan	91	38	825	1600	-	-	-
Youquanzi	91.3	38.3	425	1450	4350	-	-
Eboliang	92.6	38.6	450	1700	-	-	-
Dayoumiao	93.1	38.6	450	750	1325	-	-
	Location		Cenozoic Cumulative Thicknesses				
	Longitude	Latitude	Quaternary	Pliocene	Miocene	Oligocene	Cretaceous
Hexi Corridor Basin							
Huashen	98.35	40.16	105.5	1046	1147	1197	-
Huatan	98.08	40	135	789	1013	-	-
Youtan	102.7	38.5	336.5	-	600	-	1247.5
Jiaonan	102.7	38.7	27	-	442	-	1619

Dash means that no information was available either because of imprecise dating (Hexi basin) or shallow drilling (Qaidam). Quaternary information for Qaidam was not available directly in logs, except at Yanhu (700 m).

Table 4. Data Type and References Used in This Study

Basin	Data Type	Source
Qaidam	Neogene and Quaternary (1:2,500,000; 1000)	*Sun and Leibo* [1984]
	Oligo-Miocene (1:10,000,000; 200)	*Xu* [1985]
	Pliocene (1:10,000,000; 200)	*Xu* [1985]
	Quaternary (1:10,000,000; 200)	*Xu* [1985]
	Eight stratigraphic columns	*Xu* [1985]
Hexi	Base of Cretaceous (1:2,500,000; 500)	*Sun and Leibo* [1984]
	Quaternary (1:2,500,000; 100)	*Zhu* [1990]
	Four drill logs	TOTAL CFP
Gong He	Quaternary (200)	*Ma* [1989]

Numbers in parentheses indicate map scale and uncertainty (in meters) assumed for calculations. TOTAL CFP is the Petroleum company TOTAL Companie Française des Pétroles.

low values of $\overline{\rho}$ because of the presence of biogenous silica or of siliceous ooze in the sedimentary column [*Davies et al.*, 1995].

Neither in the Qaidam nor Hexi basins, unfortunately, are the two variables $\rho(z)$ or $\omega(z)$ available. To alleviate this problem, we used the general solidity-depth curves ($S(z) = 1 - \omega(z)$) for shales undercompacted shales and sandstones given by *Baldwin and Butler* [1985] with their respective range of uncertainty (Figure 4) : for normal shale

$$S_f(z) = \left(\frac{z}{6020}\right)^{1/6\,35} \tag{3}$$

for undercompacted shale

$$S_f(z) = \left(\frac{z}{15000}\right)^{1/8} \tag{4}$$

for coarse sediments

$$S_c(z) = 1 - 0.49\exp\left(\frac{-z}{3700}\right) \tag{5}$$

and averaged these three curves by an exponential solidity-depth curve:

$$S_g(z) = 1 - 0.43\exp\left(-\frac{z}{3014}\right) \tag{6}$$

The uncertainty linked to estimating the grain thickness with this solidity-depth relationship is about 20% (shading on Figure 4). Equation (1) becomes:

$$M(\Delta t) = \int_{z_1}^{z_2} \overline{\rho}\left[1 - 0.43\exp\left(-\frac{z}{3014}\right)\right] dz \tag{7}$$

which yields the mass M accumulated at any point during a time interval Δt, knowing the present-day thickness of strata $(z_2 - z_1)$. Because $\overline{\rho}$ is assumed to be constant, compacted volumes of rocks, also known as solid phase volumes, are equivalent to mass. Hence we will hereafter refer to solid phase when giving local (mm yr^{-1}) and regional (km^3 myr^{-1}) accumulation rates, equivalent to mass accumulation rates.

3.3. Mass Balance Procedure

Given an isopach and a stratigraphic column, the regionally balanced reconstruction of strata in the column and above the isopach can be done by assuming that the relative thickness of each strata defined in one column is constant everywhere in the vicinity of that column. In other words, we infer that the proportions of the different stratigraphic formations at one data point (drill hole) hold over a certain area around it (Figure 5). Given the total depositional area and all the sites where a ratio is computed, the vicinities are defined using a nearest neighbor method. The isopach map considered in the case of the Qaidam gives the thickness of sediments deposited since the beginning of the Neogene. It was digitized and interpolated on a regular 5-min arc resolution grid. The bounding surfaces of the different stratas are then reconstructed by calculating at each point of the grid the product between the thickness given by the isopach and the proportion of sediments calculated from the column [*Métivier and Gaudemer*, 1997].

If M drill hole measurements are available, we divide the basin into M domains, according to a criterion of minimum distance to drill hole sites. At each site (x_o, y_o) the accumulation of N layers of thickness $h_i(x_o, y_o)$, for $i = 1, ..., N$ during the Neogene leads to:

$$\begin{gathered}\sum_{i=1}^{N} h_i(x_o, y_o) = H(x_o, y_o) \\ \text{for } i = 1, ..., N \text{ and } J = 1, ..., M\end{gathered} \tag{8}$$

We then define at each site the relative thickness of each strata according to:

$$R_i = \frac{h_i(x_o, y_o)}{H(x_o, y_o)}, \text{ for } i = 1 \ldots N \tag{9}$$

Eventually we assume the relative thickness defined at one drill-site to be constant over the corresponding domain, hence:

Figure 3. Map showing sampling density of data digitized and used to compute mass balance. Numbers refer to stratigraphic sections in Figure 2.

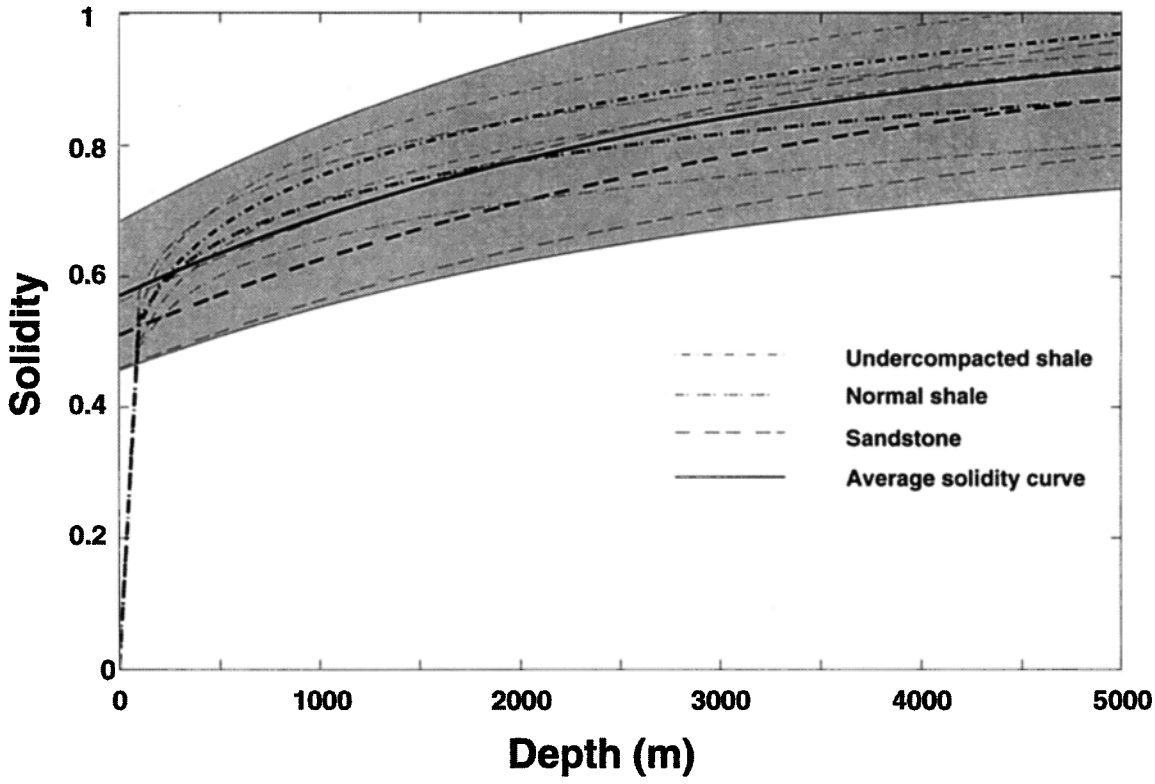

Figure 4. Solidity curves for sandstones, normal shales, and undercompacted shales from *Baldwin and Butler* [1985] and average solidity curve used in this study (equation (6)). Thinner lines give uncertainties for curves of *Baldwin and Butler* [1985]; shaded area shows uncertainty envelope for average solidity curve.

$$h_{ij}(x,y) = R_{ij}H(x,y) \qquad (10)$$

for $i = 1, \ldots, N$ and for $j = 1, \ldots, M$

The same reconstruction can be done using geologic cross sections and digitized isopachs. In the case of the Hexi Corridor, we defined four vicinities, one for each of the drill sites available; while in the more complex case of the Qaidam, we used the digitized sets available for the different epochs together with the eight stratigraphic columns to compute the proportion of each strata at each grid node.

Equation (10) gives the general formula for the reconstruction of N different stratigraphic layers provided that the cumulative thickness of such layers everywhere in the depositional area, given by isopach maps digitized and interpolated on a regular grid, and the thickness/time ratio at M different points, given either by drill holes, cross sections or even by isopach maps, are known. This is the case in the Qaidam, where we have several maps spanning the period of interest. Thus our reconstruction has a maximum resolution given by the grid spacing. Ideally, if one drill log were available at each grid point the problem would be completely determined, and the reconstruction would be ascertained. Thus the reconstruction technique can be demonstrated to be mathematically exact when tending toward the limit where one drill hole exists at each point in space. Details of the uncertainty calculation that can be derived from differential calculus are discussed by *Métivier and Gaudemer* [1997] and given in appendix A.

4. Results and Interpretation

4.1. Analysis

The total volumes of the Neogene and Quaternary solid phase are: 415,000 ± 160,000 km^3 for the Qaidam basin and 23,000 ± 16,000 km^3 for the Hexi Corridor. From the other data sets, namely, drill holes and other digitized isopachs, we compute at each grid point the proportion of the sediments that accumulated during each of the following periods: Quaternary (1.6–0 Ma), upper Pliocene (3.4–1.6 Ma), lower Pliocene (5.3–3.4 Ma), upper Miocene (11.2–5.3 Ma), and lower to middle Miocene (23.7–11.2 Ma). The Oligocene thicknesses were also reconstructed by extrapolation of the proportions of sediments from the Neogene and Quaternary

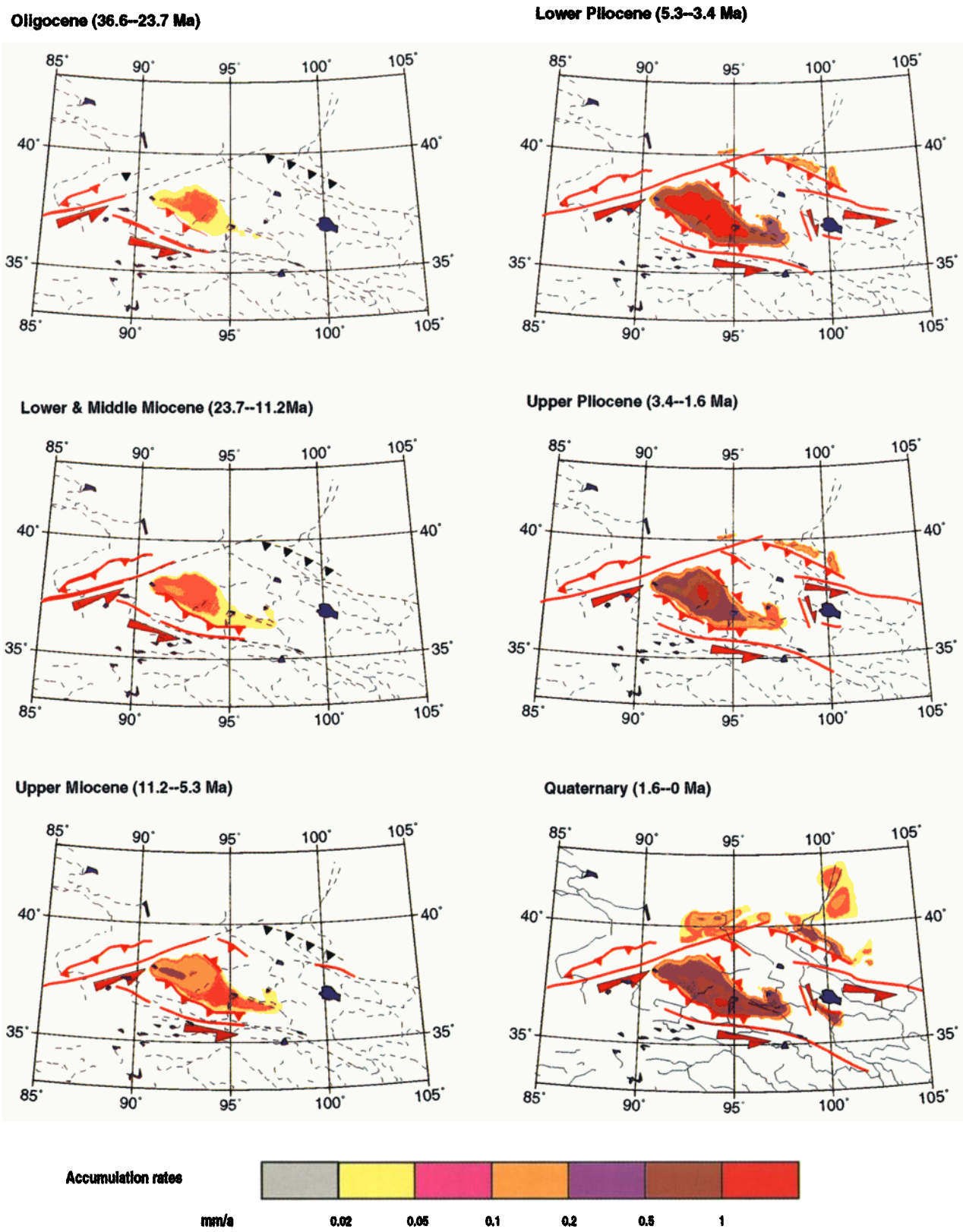

Plate 2. Accumulation rates in Qaidam and Hexi Corridor during six time intervals. Rates are given in mm yr^{-1} of solid phase. Quaternary accumulation rates in Gong He basin are given for comparison purposes. Present-day drainage (blue), and active faults (black dotted lines) serve as reference frame. Interpretation of fault propagation consistent with the model of NE Tibetan tectonics is given in red.

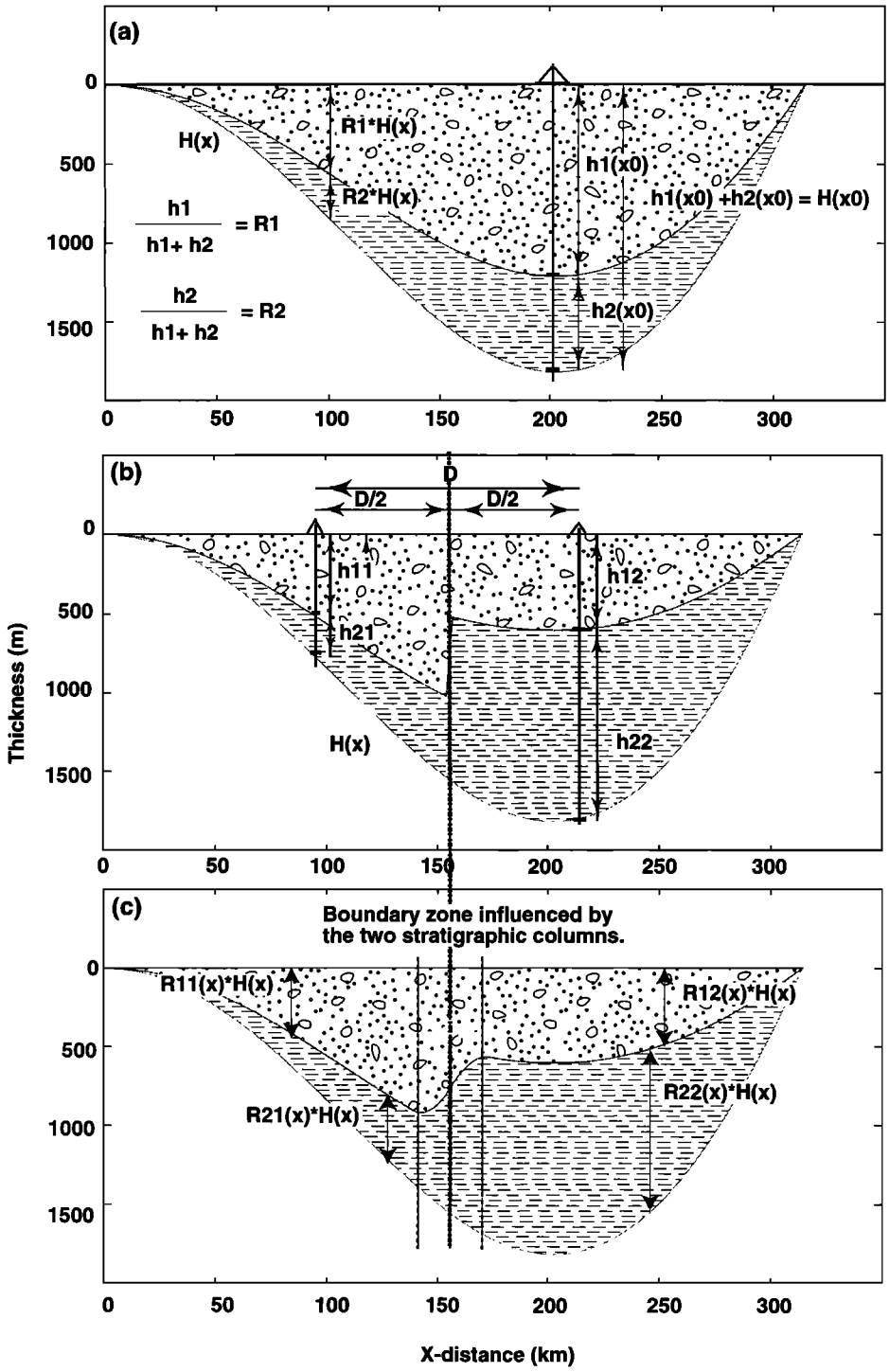

Figure 5. (a) Two-dimensional reconstruction of two sedimentary layers from one isopach and one drill hole. (b) and (c) Same as in Figure 5a for one isopach and two drill holes, with smoothing of transition zone. Variables are defined in text.

base grid. Eventually, after deriving the solid phase, the mass accumulated at each grid point in the basin during the six time intervals selected can be computed (Plate 2). The final mass balance including grain volumes, mass, and linear accumulation rates for the Qaidam basin and Hexi Corridor is shown in Table 5 with the corresponding uncertainties.

The sedimentation pattern in the Qaidam basin (Plate 2) reveals several robust trends. The basin history can be divided into two major periods: before and after the

Table 5. Volume Balance and Average Accumulation Rates in Qaidam, Hexi Corridor, and Gong He Basins

Time Period, Ma	Gong He, km^3	Gong He, mm yr^{-1}	He Xi, km^3	He Xi, mm yr^{-1}	Qaidam, km^3	Qaidam, mm yr^{-1}	Maxima, mm yr^{-1}
1.6	2,800	0.18	16,000	0.47 (0.06)	67,000	0.41	1.07
	± 400	± 0.03	± 12600	± 0.36 (0.05)	± 26,000	± 0.16	± 0.37
3.4					59,000	0.32	1.1
					± 22,000	± 0.12	± 0.32
5.3			4,500	0.16	146,000	0.74	1.59
			± 2,700	± 0.09	± 56,000	± 0.29	± 0.49
11.2					49,000	0.08	0.23
					± 20,000	± 0.03	± 0.07
23.7			2,000	0.07	53,000	0.04	0.11
			± 1000	± 0.03	± 22,000	± 0.02	± 0.03
36.6			250	0.01	41,000	0.03	0.07
			± 100	± 0.00	± 16,000	± 0.01	± 0.02
Total volume	2,600		22,750		415,000		
	± 400		± 16,400		± 162,000		

Volume of sediments accumulated in front of Qilian Shan reached maximum value during Quaternary, but this rise is coeval with a change in depositional surface area. Total volume accumulated therefore rises while local accumulation rates may decrease. Numbers in parentheses are accumulation rates derived using Quaternary depositional area. This example demonstrates usefulness of mass balance. Correlative uncertainties are given in second row for each time period.

onset of the Pliocene. Pre-Pliocene sedimentation rates over most of the basin are less than 0.1 mm yr^{-1}. Maximum rates are $\leq$ 0.5 mm yr^{-1} in the west at the front of the Kunlun Shan. After 5 Ma such rates rise everywhere above 0.1 mm yr^{-1} with peak values as high as 1.5 mm yr^{-1} during the lower Pliocene. After the lower Pliocene the maximum sedimentation rates decrease, and the surface of the depocenter is reduced and located around the center of the basin ($\sim$ 93°E and 37°N). From the upper Pliocene to the Quaternary this depocenter shifts southeastward. The maximum sedimentation rates rise again, although they do not reach the values attained in the lower Pliocene. Overall, since the beginning of the Oligocene, when sedimentation remained confined in the western part of the basin near the Altyn Tagh fault zone, there seems to have been a tendency for southeastward shifting of the depocenter. In the Hexi corridor a clear rise in the sedimentation rates also seems to occur in the Pliocene.

In terms of average accumulation rates in km^3 myr^{-1} over the entire basins (Figure 6 and Table 5), the sedimentation pattern in the Qaidam shows that the average rates of accumulation rise during the middle-upper Miocene. Average rates are twice those of the Oligocene (Figure 6 and Table 5). In the Qaidam basin a spectacular increase, by nearly one order of magnitude, takes place at the end of the Miocene (Table 5 and Figure 6) . Maximum accumulation occurs during the Pliocene. In the Hexi Corridor, maximum accumulation occurs during the Quaternary. The general trend of the average accumulation curves in the Qaidam and Hexi basins (dotted lines on Figure 6) shows a shift in time (Δt_{prop}) of the onset of rapid accumulation rates (arrows on Figure 6). The acceleration of accumulation in the Hexi corridor postdates that in the Qaidam basin by $\Delta t_{prop} \sim 5$ Myr.

4.2. Comparison With Regional Tectonics

Integrating of our results with the regional mechanism of deformation proposed by *Meyer et al.* [1998] yields further insight into the coupling between sedimentation and tectonics. Sedimentation in elongated depressions at the front of the Kunlun and Qilian mountain ranges is consistent with flexural loading of the Qaidam and Gobi lithospheres, as required by large-scale thrusting of the ranges onto their foreland. Eastward shift of the depocenters during the Tertiary suggests eastward displacement of flexural loading of the Qaidam block by the Kunlun range. The eastward growth of thrusts from the Altyn Tagh fault that borders the basin to the west [*Meyer et al.*, 1998] thus appears to be compatible with the observed evolution of the sedimentation pattern in the Qaidam basin (Plate 2).

Curves displaying the accumulation rates in the Qaidam and Hexi basins (Figure 6) show that maximum sedimentation is diachronous. At present, the Hexi corridor basin is a foreland flexural depression. Deposition is therefore controlled by thrusting of the Qilian Shan over the Gobi platform. The sedimentary record thus suggests that the onset of thrusting in the Qilian Shan postdates that in the Kunlun Shan. This implies northeastward propagation of crustal shortening and mountain building, probably concurrent with propagation of the Altyn Tagh fault at about 100 km Myr^{-1}. Such a

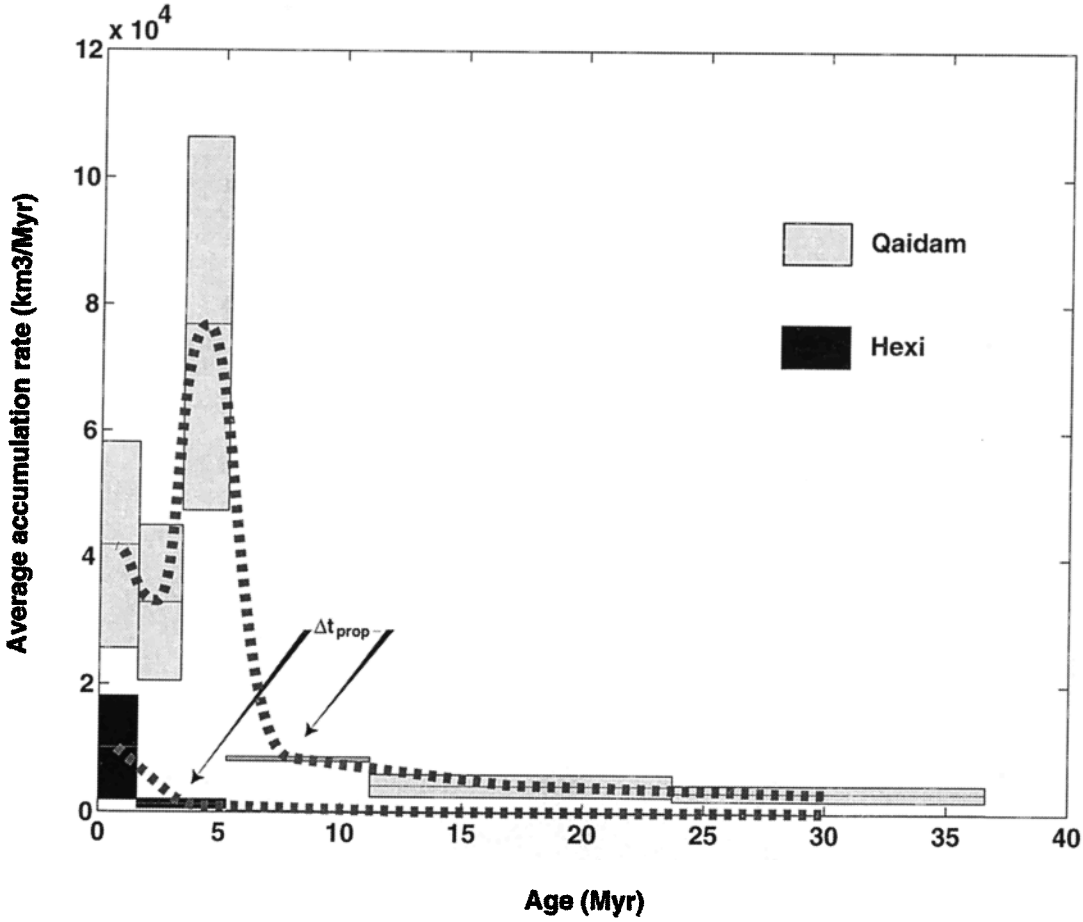

Figure 6. Average accumulation rates integrated over entire Qaidam and Hexi basins. Dotted curves, linking mid points of each period, show general trends of accumulation rates. The $\Delta t_{prop} \sim 5$ Myr shift in inflexion of Qaidam and Hexi curves as indicated by arrows yields rough estimate of propagation time of deformation from Kunlun front to Qilian Shan thrust front and hence the propagation rate of Altyn Tagh fault. Maximum accumulation rates in Qaidam correspond to damming and closure of the basin, inducing extremely rapid accumulation of sediments. Note order of magnitude difference between accumulation rates in Qaidam and in Hexi Corridor.

rate, indeed, corresponds to the approximate length of the Altyn Tagh fault between the Kunlun and Qilian Shan divided by $\Delta t_{prop} \sim 5$ Myr (Plate 2 and Figure 6).

The basinwide, approximately tenfold Pliocene increase of the accumulation rates in the Qaidam corresponds to the establishment of a vast lacustrine area [*Bally et al.*, 1986; *Gu and Di*, 1989]. This implies that the river discharge could not escape the mountain-surrounded depression but accumulated to form a large lake. Such a situation suggests closure of existing drainage outlets and damming of the catchment. If the yield carried by the streams remained roughly constant at that time, this damming process must have led to very rapid infilling of the basin. The existence of rapid accumulation rates resulting in thick deposits topped by remarkably smooth and flat surfaces is clear in the field. Figure 7a for instance, shows the thick Quaternary infill of the Gong He basin, which produced the flat topography shown in Figure 7b, while Plate 2 shows the accumulation rates in that basin during the Quaternary.

Overall, our results are thus in agreement with the deformation and growth mechanism proposed by *Meyer* [1991], *Meyer et al.* [1998] (Figure 1) and *Tapponnier et al.* [1990]. They do not rule out alternative models that would include diachronous deformation north of Tibet [e.g., *England and Houseman*, 1986], but such models lack predictive power concerning topography, erosion and sedimention, and deformation chronology at the scale needed for a test by field mesurements.

4.3. Damming of the Catchments and "Bathtub" Basin Infilling

The quantitative reconstruction performed allows us to address in greater detail problems such as the catchment damming mechanism, the time needed to fill a

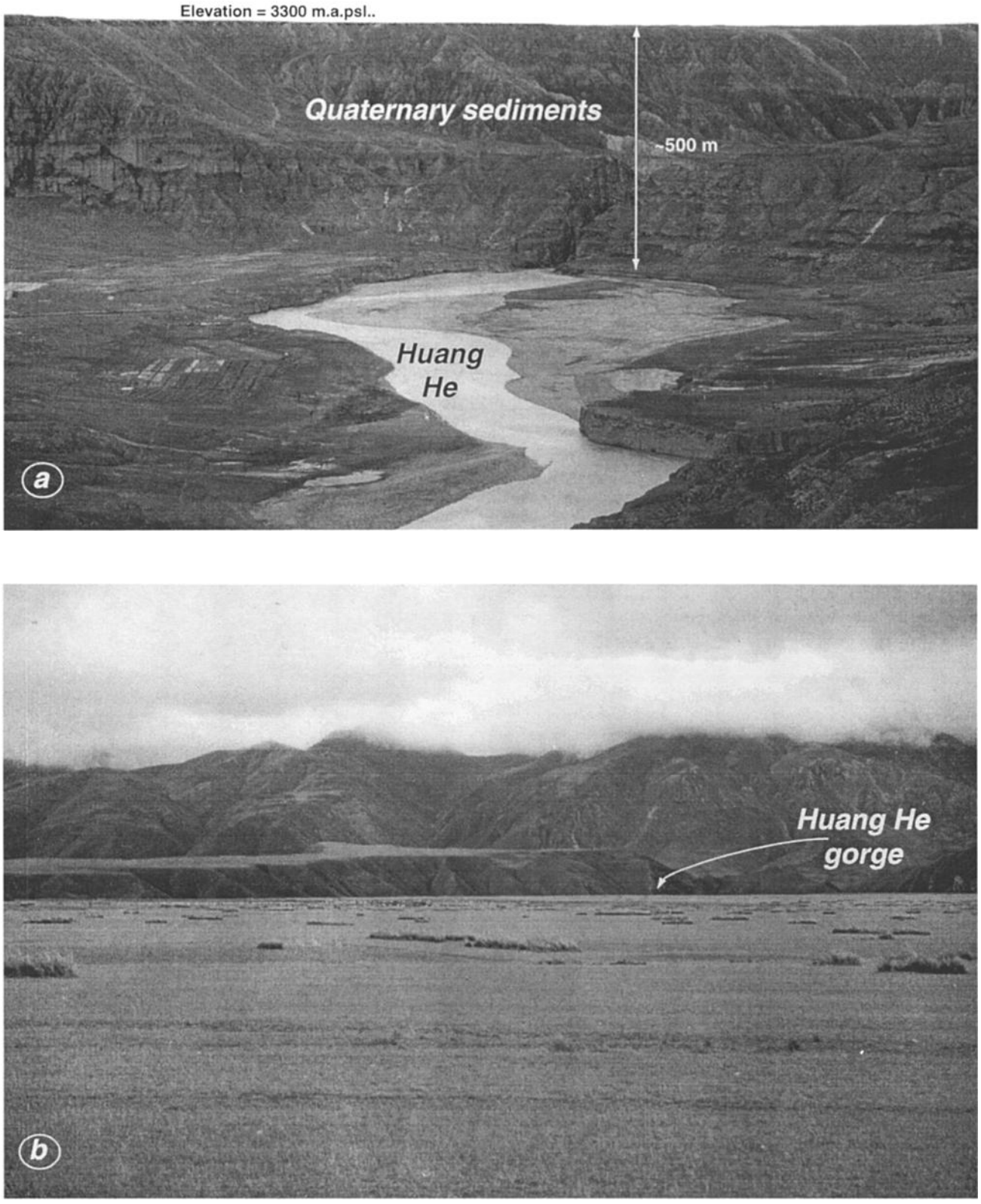

Figure 7. (a) Photograph taken (from SW looking to NE) of Huang He gorge south of Gong He basin (inset, Plate 1), showing large thickness of late Quaternary deposits. Note smooth flat surface of topography above deposits. (b) Photo taken from above Huang He gorge, standing on top of Quaternary sediment pile and showing remarkable flatness of topography induced by basin infilling.

basin and the time needed to construct successive plateaus by a combination of thrusting and basin infilling. Several processes may have led to damming of the Qaidam basin. The simplest one, depicted in Figure 1, is the rise of mountain ranges north of the basin on thrust ramps splaying from the Altyn Tagh fault. At a more detailed level, part of the deformation east of the Qaidam is accommodated by NW-SE right-lateral faults such as the Haiyen and Wenquan faults [Plate 1 ; *Gaudemer et al.*, 1995 ; *Van der Woerd*, 1998]. Dextral movement along these faults accomodates counterclockwise rotations of crustal blocks induced by regional N30°E shortening and by sinistral shear between the Altyn Tagh, Kunlun, and Haiyuan faults [*Gaudemer et al.* 1995]. Pliocene slip on the Wenquan fault [*Gaudemer et al.*, 1995] might have induced closure of the Qaidam catchment, the resulting transpression and lateral shift having recently created the subtle drainage divide between the Qaidam and the Gong He basin, a foreland flexural depression associated whith the uplift of the Qinghai Nan Shan [*Van der Woerd*, 1998]. The Wenquan fault has a total offset of $\sim$ 10–15 km, and block rotation kinematics imply that it moves at $\sim$ 3–5 mm yr^{-1} [*Gaudemer et al.*, 1995]. Hence inception of motion on it might have occurred in the Pliocene, roughly at the time when sediment deposition increased markedly in the Qaidam. Prior to this, the Qaidam basin would have been connected to the Gong He basin and might have drained into the Huang He, which now incises deeply into the sediments deposited in the southeastern part of that basin (Figure 7).

In short, the Qaidam basin might have been fed, prior to the late Miocene, by a river system collecting debris eroded from the Kunlun range, then channeled eastward through the Gong He plain to the Yellow River. Coeval uplift of the Qinghai Nan Shan ranges and right-lateral strike slip faulting along the Wenqan fault in the late Miocene would have led to the closure and rapid infilling of the basin.

Alternatively, the Kunlun rivers might have drained into the Tarim basin. Damming might then have occurred as a result of propagation of the Altyn Tagh fault and growth of both the Nan Qilian Shan north of the basin and the Altun Shan NW of the basin. Final damming might have been favored by the fact that the mountain ranges defining the northern and southern border of the Qaidam grew with convergent trends to meet at the southeastern tip of the basin, as depicted in Figures 1c and 1d.

Whatever the damming process, which may have involved a combination of the above mechanisms, the accumulation of erosion products from the dammed upper catchment of the Qaidam drainage system subsequently filled the basin, much like a bathtub (Figure 1) [*Tapponnier et al.* 1990; *Meyer et al.*, 1998]. "Bathtub" infilling may help explain not only the late Miocene–early Pliocene rise, but also the upper Pliocene and Quaternary decrease in accumulation rates. Infilling induces topographic rise of the basin base level. Thus the process acts as its own moderator by a feedback mechanism in which filling of a basin induces a diminution of the volume of rocks fed by erosion into it. Recall that, as shown by numerous experimental studies and field measurements [*Milos*, 1980; *Slingerland et al.*, 1994], erosion is, on a local scale, a highly dependent function of slope and, on a regional scale, dependent on the average elevation of the drainage area above the base level [*Ahnert*, 1970; *Pinet and Souriau*, 1988]. Eventually, note that this bathtub scenario is in excellent agreement with the wide extension of lacustrine and deltaic facies that cover most of the Qaidam basin during the late Miocene to Pliocene periods [*Chen and Bowler*, 1986].

4.4. Uplift and Sedimentation Rates

One may ask further how much time bathtub infilling might take to raise the surface of the Qaidam catchment ($\sim$ 250,000 km^2) to an average elevation comparable to that of Tibet $\sim$ 4900 $\pm$ 100 m [*Defense Mapping Agency*, 1992]. One must distinguish two types of uplift. In the mountain ranges surrounding the Qaidam basin, topographic uplift results from thrusting and folding. Within the basin, infilling produces uplift of the depositional surface. Neither such mountain uplift or basin infill, commonly called uplift of rocks, however, is the same as topographic uplift because of isostatic compensation. Let $\Delta u/\Delta t$ be the rate of basin filling and let C be the compensation ratio accounting for flexure and isostasy; the resulting topographic uplift $\Delta h/\Delta t$ is

$$\frac{\Delta h}{\Delta t} = C\frac{\Delta u}{\Delta t} \tag{11}$$

C varies between two end-members, local isostasy and flexural loading. Assuming local isostasy,

$$C = \frac{\rho_m - \rho_c}{\rho_m} \tag{12}$$

where ρ_m and ρ_c are densities of mantle and crustal rocks, respectively. For usual values of 3300 and 2700 kg m^{-3},

$$C \sim 0.18 \tag{13}$$

In the case of a sedimentary infill, one must estimate the infill in terms of either decompacted or fully compacted rocks so that density remains constant with depth. Here we use the mass equivalent, that is, compacted rocks or solid phase volumes and thicknesses.

Assuming flexural loading of an infinitely rigid plate (the flexural rigidity $D \to \infty$),

$$C = 1 \tag{14}$$

Between these two extremes, it is difficult to estimate the value of C unless both rock and topographic uplift are known. In that case (11) reduces to

$$C = \frac{\Delta h}{\Delta u} \tag{15}$$

where Δh and Δu are the finite rock infill and topographic uplift integrated over a time period Δt. Equation (15) is useful because it integrates local and regional (flexural) components and gives access to the resulting compensation of uplift. In the case of NE Tibet, thrusting is mostly directed toward the northeast [*Meyer et al.*, 1998], and uplift takes place relative to a regional base level that corresponds to the elevation of the Gobi-Ala Shan Platform. The present-day elevation of that platform is of the order of 1400 m [*Defense Mapping Agency*, 1992]. Strong sedimentation in the Qaidam basin takes place at the end of the Miocene. The basin has remained a depositional area since the end of the Permian and thus has always been a lowland relative to neighboring reliefs. Ranges north of the Qaidam, such as the Sule Nan and Tang He Nan Shan, are currently rising fast, carbon dating of deformed terraces suggest rates of several mm yr^{-1}, [*Van der Woerd*, 1998], which implies that they are only a few million years old. Thus it is reasonable to assume that the Qaidam basin was not higher than the Gobi-Ala Shan Platform at the beginning of the Pliocene, when increase in the sedimentation rates took place.

The elevation difference between the present-day Qaidam and the Gobi is $\Delta h \sim 1300$ m. Assuming that this elevation difference was achieved since closure of the Qaidam catchment ~ 5 Ma, ~ 2700 m of solid infill were necessary. This value corresponds to the volume of Plio-Quaternary solid phase infill divided by the surface of the basin (Tables 1 and 5). Using (15), we may thus estimate directly the compensation ratio in the Qaidam basin:

$$C_Q = 1300/2700 \sim 0.48 \tag{16}$$

This is more than twice the usual compensation ratio under local isostasy. Such a difference may be due either to the initial density of the sediments before compaction, which can be much less than the average crustal density of rocks, especially for rapidly accumulating argillaceous sediments [e.g., *Baldwin and Butler*, 1985], or to the rigidity of the lithosphere beneath the basin. Note that such a high compensation ratio is consistent with seismic results indicating thinner crust under the Qaidam than under the Qilian Shan [e.g., *Wittlinger et al.*, 1996]. To raise farther the surface of the Qaidam basin from its present-day elevation to 4900 m, at the level of the plains south of the Kunlun [*Defense Mapping Agency*, 1992], a base level uplift by sediment infilling of

$$\Delta h_{\text{fill}} \sim 2200 \text{ m} \tag{17}$$

is needed. Using (11) and (16), the equivalent solid phase infill required is

$$\Delta u_{\text{fill}} = \frac{\Delta h_{\text{fill}}}{C} \sim 4600 \text{ m} \tag{18}$$

From our mass balance we can derive the average solid phase infill rate ($\Delta h_s/\Delta t$) of the Qaidam basin. Using the total volume accumulated since ~ 5 Ma (Table 5) and dividing it by the depositional area (Table 1), we obtain

$$\frac{\Delta h_s}{\Delta t} \sim 0.5 \text{ mmyr}^{-1} \tag{19}$$

Assuming, to a first order, such a rate to remain constant, the time needed to fill the Qaidam basin up to the elevation of the Qangtang (4900 m) would be

$$\Delta t_{\text{fill}} = \Delta u_{\text{fill}} \left(\frac{\Delta h_s}{\Delta t} \right)^{-1} \sim 9 \text{ Myr} \tag{20}$$

The total time needed to form a 250,000 km^2 broad, high plateau comprising the Qaidam basin and the ranges drained by its catchment also includes the period since onset of tectonic thrusting. The volumetric accumulation rates double between the early and late Miocene around 11 Ma (Table 5). Thrusting had been going on for at least 5 Myr before the sharp rise in accumulation rate, since seismic sections show such thrusting to postdate Oligocene deposition and predate Pliocene deposition [*Bally et al.*, 1986]. Mountain building south of the Qaidam thus probably started during the middle-upper Miocene, between 15 and 5 Ma, in keeping with the onset of volcanism south of the Kunlun [*Tapponnier et al.*, 1990; *Meyer*, 1991; *Meyer et al.*, 1998]. Hence the time required to transform the Qaidam and its mountain rims into a 250,000 km^2 broad plateau is of the the order of

$$24 \text{ Myr} \geq \Delta t_{\text{f}} \geq 14 \text{ Myr} \tag{21}$$

As uplift and thrusting propagate along with the Altyn Tagh fault, parallel building of small plateaus at different stages of their evolution may occur simultaneously (Figure 1). A new range and its foreland basin may begin to form in the NE while older basins undergo damming to the SE, and yet farther SE, bathtub infilling of even older mountain-locked basins is near completion. Given the northeastward propagation time ($\Delta t_{\text{prop}} \sim 5$ Myr) inferred before from the delay in rapid accumulation rate onset between the Qaidam and Hexi basins and the surface of the now internally drained part of Qangtang ($\sim 725{,}000$ km^2), approximately 3 times that of the Qaidam catchment, a rough first-order dimensional analysis allows us to estimate the onset of north central Tibet's growth by schematically modeling its formation as the successive, partly coeval growth

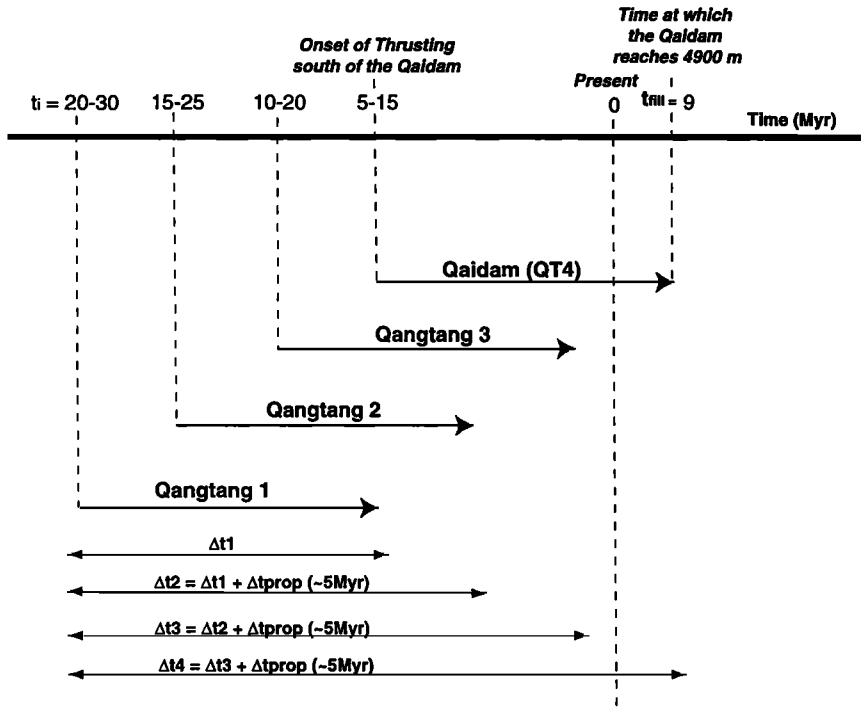

Figure 8. Time-span of Qangtang growth consistent with mechanism in Figure 1. Northeastward propagation of deformation onset is ~ 5 Myr (Figure 6), and each period lasts 5-15 Myr. Knowing history of Qaidam basin and drainage (QT4) makes it possible to go back to t_0, onset time of northeastward growth of Qangtang.

of three subplateaus comparable in size to the Qaidam catchment (QT1, QT2, and QT3, Figure 8). The timing of such a process takes the form of an arithmetic series (Figure 8)

$$\Delta t_n = \Delta t_{n-1} + \Delta t_{\text{prop}} \quad n = 1, \ldots, 3 \tag{22}$$

where Δt_n is the time needed to form the n first sub-Tibets (Figures 1 and 8). Equation (22) can be developed into

$$\begin{aligned} \Delta t_n &= \Delta t_{n-1} + \Delta t_{\text{prop}} \\ &\vdots \quad\quad \vdots \\ \Delta t_1 &= \Delta t_f + \Delta t_{\text{prop}} \end{aligned} \tag{23}$$

which leads to

$$\Delta t_n = \Delta t_f + 3\Delta t_{\text{prop}} \tag{24}$$

Δt_n being the time span between t_0, onset time of Qangtang growth, and t_{fill}, time of complete infilling of the Qaidam One obtains

$$t_0 = \Delta t_f + 3 \times \Delta t_{\text{prop}} - t_{\text{fill}} \tag{25}$$

$$20 \text{ Ma} \leq t_0 \leq 30 \text{ Ma} \tag{26}$$

a total time that amounts to about half the duration of the India-Asia collision.

5. Summary and Conclusion

In this study we have used isopach maps and drill logs to reconstruct the volumes and masses accumulated in two of the largest sedimentary basins of NE Tibet: the Qaidam and Hexi Corridor. The spatial and temporal history of mass accumulation is in good agreement with a mechanism of strike-slip driven, northeastward migration of overthrusting and uplift south of the NE termination of the propagating Altyn Tagh fault [*Tapponnier et al.*, 1990; *Meyer*, 1991; *Meyer et al.*, 1998]. Growth of such large faults induces successive closure of vast, flat, depositional areas born in part as flexural and in part as piggyback basins at the foot of and between active mountain ranges. Final basin closure induces very rapid and uniform filling of such depressions, allowing for the formation of several tens of thousands of square kilometers wide, high and flat, internally drained plateaus. Such plateaus remain surrounded by modest crests, remnants of the mountain belts once responsible for damming the original catchments. Quantitative assessment of this bathtub scenario of sedimentary filling implies that it is possible to transform the Qaidam and its catchment into a flat high plateau over a rather short time. We infer the onset of northeastward growth of north central Tibet to have taken place about 20-30 Ma using a simple first-order arithmetic propagation model along the Altyn Tagh left-lateral strike-slip fault.

Following *Meyer et al.* [1998] and *Tapponnier et al.* [1990] we believe this simple mechanism to have played a fundamental role in building the remarkably flat morphology of the high, north central Tibet plateau.

Appendix A: Uncertainties in Mass Balance Calculations

From (10) one can derive the relationship between the uncertainty assumed for the isopach database δH and the uncertainty at the ith site:

$$\delta h_i(x,y) = R_{ij}\delta H(x,y) \tag{27}$$

Combining this uncertainty and that linked with the solidity curve in the compaction process (subscript g for grain thickness) of the ith strata leads to

$$h_{g,i}(x,y) = \int_{z_i(x,y)}^{z_i(x,y)+h_i(x,y)+\delta h_i(x,y)} (S(u)+\delta S(u))du \tag{28}$$

where z_i is the depth of the top of the ith strata. For the purpose of simplifying the form of the equations we thereafter drop the (x,y) position index of the functions because it has no influence on the uncertainty calculus. $\delta S(u)$ is assumed to be $0.2S(u)$; thus we get

$$h_{g,i} = \int_{z_i}^{z_i+h_i+\delta h_i} S(u)du + 0.2\int_{z_i}^{z_i+h_i} S(u)du \tag{29}$$

Because $z_i = z_{i-1}+h_{i-1}$, there is an uncertainty in position of the top of the ith strata of the form

$$z_i = z_{i-1} + h_{i-1} + \delta h_{i-1} \tag{30}$$

This arithmetic series once propagated to the top of the first strata leads to

$$z_i = \sum_1^{i-1} h_l + \sum_1^{i-1} \delta h_l \tag{31}$$

Equation (29) then becomes :

$$h_{g,i} = \int_{z_i+\sum_1^{i-1}\delta h_l}^{z_i+h_i+\sum_1^{i}\delta h_l} S(u)du + 0.2\int_{z_i}^{z_i+h_i} S(u)du \tag{32}$$

Developing the first integral of the right-hand side of (29) to the first order leads to

$$\begin{aligned} h_{g,i} &= \int_{z_i}^{z_i+h_i} S(u)du + \delta h_i S(z_i) \\ &\quad + \sum_1^{i-1}\delta h_l\,(S(z_i+h_i)-S(z_i)) \\ &\quad + 0.2\int_{z_i(x)}^{z_i(x)+h_i(x)} S(u)du \end{aligned} \tag{33}$$

We will thus assume the uncertainty in the grain thickness to be

$$\delta h_{g,i} = \left|\delta h_i S(z_i) + \sum_1^{i-1}\delta h_l[S(z_i+h_i)-S(z_i)] + 0.2\int_{z_i(x)}^{z_i(x)+h_i(x)} S(u)du\right| \tag{34}$$

The uncertainty boxes shown in Figure 6 thus correspond to the surface integral of (34).

Appendix B: Influence of Dating Uncertainty on Significance of Results

Erroneous dating of the strata, especially of those marking the onset of high rates of accumulation, may bias the reconstruction. In the Qaidam, in particular, the age of the Youshashan Formation is controversial. *Bally et al.* [1986] place the entire formation in the Pliocene, while *Xu* [1985], who we follow, places the lower part of the Formation in the late Miocene age and places the upper part in the lower Pliocene.

Assuming all the Youshashan Formation to be of Pliocene age would further increase the already huge deposition rates we find. How would the reconstruction results be affected if both age estimates were off by more than 100% ? To test the reliability of the change in the sedimentation pattern at 5 Myr, we calculated the hypothetical time t_h at which the average rates of accumulation for the periods before and after the onset of deposition of the upper Youshashan Formation would become equal. From Tables 3 and 5 we obtain two volumes of rocks: (1) The first one $V_1 \sim 143,000$ km^3 corresponds to the accumulation between 36 Ma and t_h. (2) The second one $V_2 \sim 272,000$ km^3 corresponds to the sediment accumulation between t_h and present.

Equivalence in the average accumulation rates leads to

$$\frac{V_1}{36-t_h} = \frac{V_2}{t_h} \tag{35}$$

From (35), we obtain

$$t_h = \frac{36V_2}{V_1+V_2} = 23.6 \text{ Ma} \tag{36}$$

This result means that unless there is 470% uncertainty in the dating of the limit between the upper and lower Youshashan Formation, the volume accumulated after that limit is significantly greater than the volume accumulated before. Hence, although uncertainty in dating of such continental strata might be of the order of a couple of millions of years, the sedimentary signal in the upper Tertiary and Quaternary is so strong that the results and correlative uncertainties obtained can be regarded as robust.

Acknowledgments. Michel Klein and TOTAL CFP are greatfully acknowledged for providing some of the data used in this study. We acknowledge discussions with J.Van der Woerd and P. Molnar. After what seemed to be an everlasting review process, this paper eventually benefitted from fruitfull comments by A. Schlunnegger and two anonymous reviewers. This is IPGP contribution N 1563 and INSU PROSE contribution N 114.

References

Ahnert, F., Functional relationships between denudation, relief, and uplift in large mid-latitude drainage basins, *Am. J. Sci., 268*, 243–263, 1970.

Argand, E., La tectonique de l'Asie,*Proc. Int. Geol. Cong. XIII, I*, 5, 372 pp, 1924.

Baldwin, B., and C.O. Butler, Compaction curves, *AAPG Bull., 69*, 622–626, 1985.

Bally, A., I.-M. Chou, R. Clayton, H. Eugester, and K.S. Meckel, Notes on sedimentary basins in China–Report of the American sedimentary delegation to the People's Republic of China, *Open File*

Rep., 86-327, U. S. Geol. Surv., 1986.

Bird, P., Initiation of intracontinental subduction in the Himalaya, *J. Geophys. Res., 83*, 4975–4987, 1978.

Bureau of Geology and Mineral Resources of Qinghai province, *Regional Geology of Qinghai Province*, Geol. Mem., ser. 1, 24,People's Repub. of China Minist. of Geol. and Miner. Resour., Geol. Publ., Beijing, 1991.

Burg J.-P., P. Davy, and J. Martinod, Shortnening of analogue models of the continental lithosphere: New hypothesis for the formation of the Tibetan plateau, *Tectonics, 13*, 475-483, 1995.

Chen K., and J.M. Bowler, Late Pleistocene evolution of salt lakes in the Qaidam basin, Qinghai province, China, *Palaeogeogr., Palaeoclimatol., Palaeoecol., 54*, 87–104, 1986.

Chen, Y.T., Xu, L.S., Li, X. and Zhao, M., Source process of the 1990 Gonghe, China, earthquake and tectonic stress field in the northeastern Qinghai-Xizang (Tibetan) plateau. *PAGEOPH, 146*, 697–715, 1994.

Curray, J.R., Sediment volume and mass beneath the Bay of Bengal, *Earth Planet. Sci. Lett., 125*, 371–383, 1994.

Davies, T.A., R.B. Kidd, and A.T.S. Ramsay, A time-slice approach to the history of Cenozoic sedimentation in the Indian Ocean, *Sediment. Geol., 96*, 157–179, 1995.

Defense Mapping Agency, *Digital Chart of the World*, Fairfax, Va., 1992.

England, P.C., and G. Houseman, Finite strain calculations of continental deformation, 2, Comparison with the India-Asia collision zone, J. Geophys. Res., *91*, 3664–3676, 1986.

England, P.C., and D. McKenzie, A thin viscous sheet model for continental deformation, *Geophys. J. R. Astron. Soc.*, 70, 295–321, 1982.

Fielding, E., B. Isacks, M. Barazangi, and C. Duncan, How flat is Tibet ?, *Geology, 22*, 163–167, 1994.

Gallagher, K., An examination of some uncertainties associated with estimates of sedimentation rates and tectonic subsidence, *Basin Res., 2*, 97–114, 1989.

Gaudemer, Y., P. Tapponnier, J. Van der Woerd, and B. Meyer, Block rotations, fault bending and mountain building, EUG8, Abstr. suppl. n°1, *Terra Nova Abstr., 7*, 1995.

Gong, S.W., Q.L. Wang, and J.H. Lin, Study of dislocation model and evolution characteristics of vertical displacement field of Gonghe *Ms* = 6.9 earthquake, *Acta Seismol. Sin.*, (Eng. Transl.), *6*(3), 641–648, 1993.

Gu, S., and H. Di, Mechanism of formation of the Qaidam basin and its control on petroleum, in *Chinese sedimentary Basins*, edited by Zhu, X., Elsevier, New York, 45–51, 1989.

Guo, S., Z. Chen, H. Xiang, and H. Dai, eds., *The Qilian Mountain-Hexi Corridor Active Fault System*, Seismological press, 340 pp., Beijing, 1993.

Hirn, A., M. Sapin, J.C. Lépine, E.Y. Gao, J.W. Teng, and M.R. Pandey, Himalya border of Tibet: crustal structure and variability, *Nature, 307*, 23–25, 1984.

Jin, Y., M. Mc Nutt, and Y. Zhu, Evidence from gravity and topography data for folding of Tibet, *Nature, 371*, 669–674, 1994.

Ma, X. (Ed.), *Lithospheric Dynamic Atlas of China*, China Cartogr., Beijing, 1989.

Mattauer, M., Intracontinental subduction, crust-mantle décollement and crustal-stacking wedge in the Himalayas and other collision belts, in *Collision Tectonics*, edited by M.P. Coward and A.C. Ries, Geol. Soc. Spec. Pub., *19*, 37–50, 1986.

Métivier, F., *Volumes sédimentaires et bilans de masses en Asie pendant le Cénozoïque*, Thèse de Doctorat, Université de Paris 7, 1996.

Métivier, F., and Y. Gaudemer, Mass transfer between eastern Tien Shan and adjacent basins: Constraints on regional tectonics and topography, *Geophys. J. Int., 128*, 1–18, 1997.

Meyer, B., Mécanismes des grands tremblements de terre et du raccourcissement crustal oblique au bord nord-est du Tibet, Thèse de Doctorat, Université de Paris 7, 1991.

Meyer, B., P. Tapponnier, L. Bourjot, F. Métivier, Y. Gaudemer, G. Peltzer, S. Guo, and Z. Chen, Mechanisms of active crustal thickening in Gansu, And Oblique, Strike-slip controlled northeastward growth of the Tibet plateau, *Geophys. J. Int.*, in the press, 1998.

Milos, H., *Erosion and Environment*, Environ. Sci. Appl., vol. 9, edited by A. Biswas and M.R. Biswas, Pergamon, Tarrytown, N.Y., 1980.

Molnar, P. and P. Tapponnier, Active tectonics of Tibet, *J. Geophys. Res., 83*, 5361-5375, 1978.

Molnar, P., P. England, and J. martinod, Mantle dynamics, uplift of the Tibetan plateau, and the Indian monsoon, *Rev. Geophys., 31*, 357–396, 1993.

Ni, J., and M. Barazangi, High-frequency seismic wave propagation beneath the indian shield, Himalayan arc, Tibetan plateau and surrounding regions : high uppermost mantle velocities and efficient S_n propagation beneath Tibet, *Geophys. J. R. Astron. Soc., 72*, 663–689, 1983.

Peltzer, G., P. Tapponnier, and R. Armijo, Magnitude of Late Quaternary left-lateral displacements along the north edge of Tibet, *Science, 246*, 1285–1289, 1989.

Pinet, P., and M. Souriau, Continental erosion and large-scale relief, *Tectonics, 7*, 563–582, 1988.

Powell, C. McA., and P.J. Conaghan, Plate tectonics and the Himalayas, *Earth Planet. Sci. Lett., 20*, 1–12, 1973.

Slingerland, R., J.W. Harbaugh, and K. Furlong, *Simulating Clastic Sedimentary Basins*, Prenctice-Hall, Englewood Cliffs, N.J., 1994.

Sun, D., and W. Leibo, *Tectonic Systems Map of the People's Republic of China and Adjacent Sea Area*, Cartogr. Publ., Beijing, 1984.

Tapponnier, P., G. Peltzer, and R. Armijo, On the mechanics of the collision between India and Asia, in *Collision tectonics*, edited by M.P. Coward and A.C. Ries, *Geol. Soc. Spec. Publ., 19*,115–156 1986,.

Tapponnier, P., et al., Active thrusting and folding in the Qilian Shan, and decoupling between upper crust and mantle in northeastern Tibet, *Earth Planet. Sci. Lett., 97*, 382–403, 1990.

Van der Woerd, J., *Couplage cinématique entre décrochements et chevauchements actifs dans le Nord du Tibet. Croissance du plateau Tibétain*, Thèse de Doctorat, Université Paris VII, 411pp., 1998.

Van Der Woerd, J., F.J. Ryerson, P. Tapponnier, Y. Gaudemer, R. Finkel, A. S. Mériaux, M. Caffee, G. Zhao, and Q. He, Holocene left-slip rate determined by cosmogenic surface dating on the Xidatan segment of the Kunlun Fault (Qinghai, China), *Geology, 26*(8), 695-699, 1998.

Wang, Q.M., and M.P. Coward, The Chaidam basin (NW China): formation and hydrocarbon potential, *J. Pet. Geol., 13*, 93–112, 1990.

Wang Q.M. and Coward M.P., The Jiuxi basin, Hexi Corridor, NW China: foreland structural features and hydrocarbon potential, *J. Pet. Geol., 16*, 169–182, 1993.

Wittlinger G., et al., Seismic tomography of northern Tibet and Kunlun : evidence for crustal blocks and mantle velocity contrasts, *Earth Planet. Sci. Lett., 139*, 263–269, 1996.

Xu, C., Qaidamu Basin, in *United Nations, Stratigraphic Correlation Between Sedimentary Basins of the ESCAP Region* vol. X, *ESCAP Atlas of Stratigraphy IV: People's Republic of China*; Miner. Resour. Dev. Ser., vol. 52, United Nations, New York, 1985.

Zhao, W.L., and W.J Morgan, Uplift of the tibetan plateau, *Tectonics, 4*, 359–369, 1985.

Zhu, Z. (Ed.), *Quaternary Geologic Map of the Peoples Republic of China and Adjacent Sea Area*, China Cartogr. Publ., Beijing, China, 1990.

Laboratoire de Tectonique, Institut de Physique du Globe , boite 89, 4 Place Jussieu,75252 Paris cedex 05, France.
gaudemer@ipgp.jussieu.fr,
metivier@ipgp.jussieu.fr,
meyer@ipgp.jussieu.fr,
tappon@ipgp.jussieu.fr

(Received October 7, 1996;
revised April 3, 1998;
accepted April 3, 1998.)